

Supplementary Information

Use of a cyclo-P₄ building block – A Way to Networks of Host-Guest Assemblies

Eugenia Peresykina,^a Martin Bielmeier,^a Alexander Virovets^a and Manfred Scheer^{*a}

Contents

1. General Remarks	2
2. Synthesis of the 1D [$\{\text{Cp}''\text{Ta}(\text{CO})_2(\mu_3, \eta^4: \eta^1: \eta^1\text{-P}_4)\}_2\text{Ag}]_n[\text{SbF}_6]_n$ (5) and the 3D [$\{\text{Cp}''\text{Ta}(\text{CO})_2(\mu_4, \eta^4: \eta^1: \eta^1: \eta^1\text{-P}_4)\}_2\text{Ag}]_n[\text{SbF}_6]_n$ (6) Polymers	2
3. Synthesis of the 2D Coordination Network $\text{P}_4\text{Se}_3@[\{\{\text{Cp}''\text{Ta}(\text{CO})_2(\eta^4\text{-P}_4)\}\text{Ag}\}_8(\text{NC}(\text{CH}_2)_7\text{CN})_{4.5}]_n[\text{SbF}_6]_{8n}$ (7)	3
4. X-ray Crystallography	5
4.1. One-Dimensional Polymer [$\{\text{Cp}''\text{Ta}(\text{CO})_2(\mu_3, \eta^4: \eta^1: \eta^1\text{-P}_4)\}_2\text{Ag}]_n(\text{SbF}_6)_n \cdot 0.35n(\text{CH}_2\text{Cl}_2)$ (5)	8
4.2. Three-Dimensional Polymer [$\{\text{Cp}''\text{Ta}(\text{CO})_2(\mu_4, \eta^4: \eta^1: \eta^1: \eta^1\text{-P}_4)\}_2\text{Ag}]_n(\text{SbF}_6)_n$ (6)	10
4.3. Two-Dimensional Coordination Network $\text{P}_4\text{Se}_3@[\{\{\text{Cp}''\text{Ta}(\text{CO})_2(\eta^4\text{-P}_4)\}\text{Ag}\}_8(\text{NC}(\text{CH}_2)_7\text{CN})_{4.5}]_n[\text{SbF}_6]_{8n} \cdot 3.75n(\text{CH}_2\text{Cl}_2)$ (7)	12
5. Topological Features of the Coordination Networks 6 and 7	17
References	19

1. General Remarks

All reactions were performed under an inert atmosphere of dry nitrogen or argon with standard vacuum, Schlenk and glove-box techniques. Solvents were purified, dried and degassed prior to use by standard procedures. Traces of O₂ or moisture in the inert gas were removed by leading it over a Cu/MgSO₄ catalyst, concentrated H₂SO₄, orange gel and P₂O₅ on a medium of pumice stone. Solvents were used from the solvent drying machine MB SPS-800 or dried according to standard methods and distilled prior to use. Commercially available chemicals (AgSbF₆ and NC(CH₂)₇CN) were used without further purification. [Cp''Ta(CO)₂(η⁴-P₄)] was synthesized following reported procedures.^[1]

Solution NMR spectra were recorded on either Bruker Avance 300 or 400 spectrometer. The corresponding ESI-MS spectra were acquired on a ThermoQuest Finnigan MAT TSO 7000 mass spectrometer, while elemental analyses were performed on a Vario EL III apparatus.

2. Synthesis of the 1D [(Cp''Ta(CO)₂(μ₃,η⁴:η¹:η¹-P₄)₂Ag]_n[SbF₆]_n (5) and the 3D [(Cp''Ta(CO)₂(μ₄,η⁴:η¹:η¹:η¹-P₄)₂Ag]_n[SbF₆]_n (6) Polymers

A yellow solution of **1a** (10.77 mg, 0.02 mmol) in 2 mL toluene is layered onto a colourless solution of AgSbF₆ (6.87 mg, 0.02 mmol) in 2 mL CH₂Cl₂, which is first layered with 1 mL of a mixture of CH₂Cl₂ : toluene (2 : 1). After 3 days, yellow plates of crystalline **5** are formed accompanied by a minor content of yellow octahedra of phase **6**. After complete diffusion, the mother solution is decanted; the crystals are washed with hexane and dried *in vacuo*. The product was obtained in a yield of 13 mg (68%, based on **1a**), and is soluble in CH₂Cl₂, insoluble in hexane and pentane and dissolves in CH₃CN and pyridine under fragmentation.

Yield: 13 mg (0.0136 mmol, 68%, based on **1a**) of **5** and a few crystals of **6**.

¹H NMR (298 K, CD₃CN): δ [ppm] = 1.12 (s, 18H, tBu, **1a**), 6.35 (d, 2H, C₅(tBu)₂H₃), 6.61 (s, 1H, C₅(tBu)₂H₃)

³¹P NMR (298 K, CD₃CN): δ [ppm] = 37.69 (t, 1P, P_A, **1a**), 12.18 (t, 1P, P_M, **1a**), -6.31 (dd, 2P, P_X, **1a**), AMX₂ spin system.

Elemental analysis: calculated for C₃₀H₄₂Ta₂P₈O₂AgSbF₆ (1419.96 g/mol): 25.38 C, 2.98 H, found: 25.03 C, 3.03 H

ESI-MS (CH₃CN):

Cation mode: *m/z* = 2602.7 [(Cp''Ta(CO)₂P₄)₄Ag₂SbF₆]⁺, 2064.70 [(Cp''Ta(CO)₂P₄)₃Ag₂SbF₆]⁺, 1692.91 [(Cp''Ta(CO)₁P₄)₃Ag]⁺, 1238.97 [(Cp''Ta(CO)₁P₄)₂Ag{CH₃CN}]⁺, 1182.91 (100%) [(Cp''Ta(CO)₂P₄)₂Ag]⁺, 1138.93 [(Cp''Ta(CO)₂P₄)₂Cu]⁺ (impurity), 728.95 [(Cp''Ta(CO)₂P₄)Ag{CH₃CN}]⁺, 687.93 [(Cp''Ta(CO)₂P₄)Ag{CH₃CN}]⁺, 644.95 [(Cp''Ta(CO)₂P₄)Ag]⁺, 613.17 [(Cp''Ta(CO)₂P₃)Ag]⁺;

Anion mode: *m/z* = 234.73 (100%) [SbF₆]⁻.

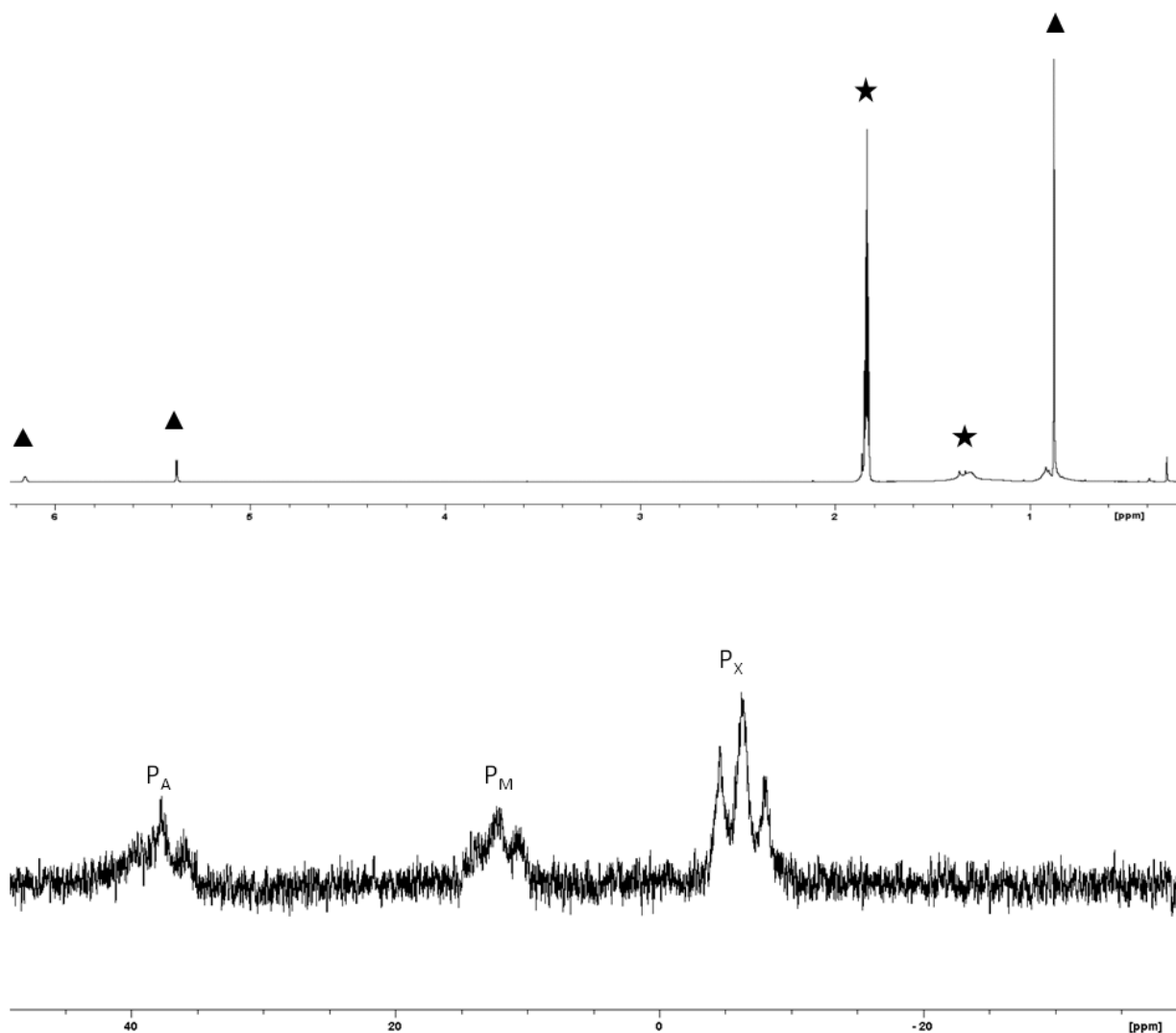


Fig. S1: ^1H NMR spectrum (top) and ^{31}P NMR spectrum (bottom) of **5** in CD_3CN at 298 K. Symbols ▲ and ★ denote signals of **1a** and solvent, respectively.

3. Synthesis of the 2D Coordination Network $\text{P}_4\text{Se}_3@[\{(\text{Cp}''\text{Ta}(\text{CO})_2(\eta^4\text{-P}_4))\text{Ag}\}_8(\text{NC}(\text{CH}_2)_7\text{CN})_{4.5}\text{]}_n[\text{SbF}_6]_{8n}$ (**7**)

A yellow solution of **1a** (10.77 mg, 0.02 mmol), P_4Se_3 (10.22 mg, 0.03 mmol)^[2] in 2 mL toluene and 0.5 mL of a 0.4 mol/L solution of $\text{NC}(\text{CH}_2)_7\text{CN}$ in 2 mL toluene (0.2 mmol) is layered over a colourless solution of AgSbF_6 (6.87 mg, 0.02 mmol) in 2 mL CH_2Cl_2 which was first layered with 1 mL of a mixture of CH_2Cl_2 and toluene (2 : 1). After complete diffusion (ca. 3 days) yellow plate-shaped crystals are formed. The mother solution is decanted; the crystals are washed with hexane and dried *in vacuo*. The product is obtained in a yield of 6 mg (0.0058 mmol, 29.1%), is sparingly soluble in CH_2Cl_2 , insoluble in hexane and pentane, and dissolves in CH_3CN and pyridine under fragmentation.

Yield: 6 mg (0.0058 mmol, 29,1% based on **1a**)

^1H NMR (298 K, CD_3CN) δ [ppm] = 1.10 (s, 18H, *t*Bu **1a**), 1.37 (m, 6H, CH_2 , linker), 1.60 (m, 4H, CH_2 , linker), 2.36 (t, 4H, CH_2 , linker), 5.44 (s, 1H, $\text{C}_5(\text{tBu})_2\text{H}_3$), 6.36 (d, 2H, $\text{C}_5(\text{tBu})_2\text{H}_3$).

³¹P NMR (298 K, CD₃CN): δ [ppm] = 36.73 (t, 1P, P_A), 11.28 (t, 1P, P_M), - 6.13 (dd, 2P, P_X), AMX₂ spin system, - 115.7 (d, 3P_{basal} P₄Se₃), no signal detected for P_{apical}.

Elemental analysis: calculated for C_{160.5}H₂₃₁Ag₈F₄₈N₉O₁₆P₃₆Sb₈Se₃Ta₈ (8541.72 g/mol) (with 3 CH₂Cl₂ and 1 toluene in the crystal lattice): 25.28 C, 2.90 H, 1.47 N, found: 25.60 C, 3.07 H, 1.58 N

ESI-MS (CH₃CN):

Cation mode: $m/z = 2604.70$ [Cp''Ta(CO)₂P₄]₄Ag₂[SbF₆]⁺, 2408.50 [Cp''Ta(CO)₂P₄]₃Ag₃[SbF₆]⁺, 2064.70 [Cp''Ta(CO)₂P₄]₃Ag₂SbF₆⁺, 1694.90 [Cp''Ta(CO)₂P₄]₂[Cp''Ta(CO)₁P₄]Ag⁺, 1182.90 (100%) [Cp''Ta(CO)₂P₄]₂Ag⁺, 795.02 [Cp''Ta(CO)₂P₄]Ag{NC(CH₂)₇CN}⁺, 767.03 [Cp''Ta(CO)₂P₄]Ag{CH₃CN}₃⁺, 726.96 [Cp''Ta(CO)₂P₄]Ag{CH₃CN}₂⁺, 685.93 [Cp''Ta(CO)₂P₄]Ag{CH₃CN}⁺, 644.90 [Cp''Ta(CO)₂P₄]Ag⁺, 602.25 [Cp''Ta(CO)₂P₄]Cu⁺ (impurity), 257.02 [Ag{NC(CH₂)₇CN}]⁺, 229.99 [Ag{CH₃CN}]₃⁺, 227.16 [Cu{CH₃CN}]₄⁺ (impurity), 213.05 [Cu{NC(CH₂)₇CN}]⁺ (impurity);

Anion mode: $m/z = 234.67$ (100%) [SbF₆]⁻.

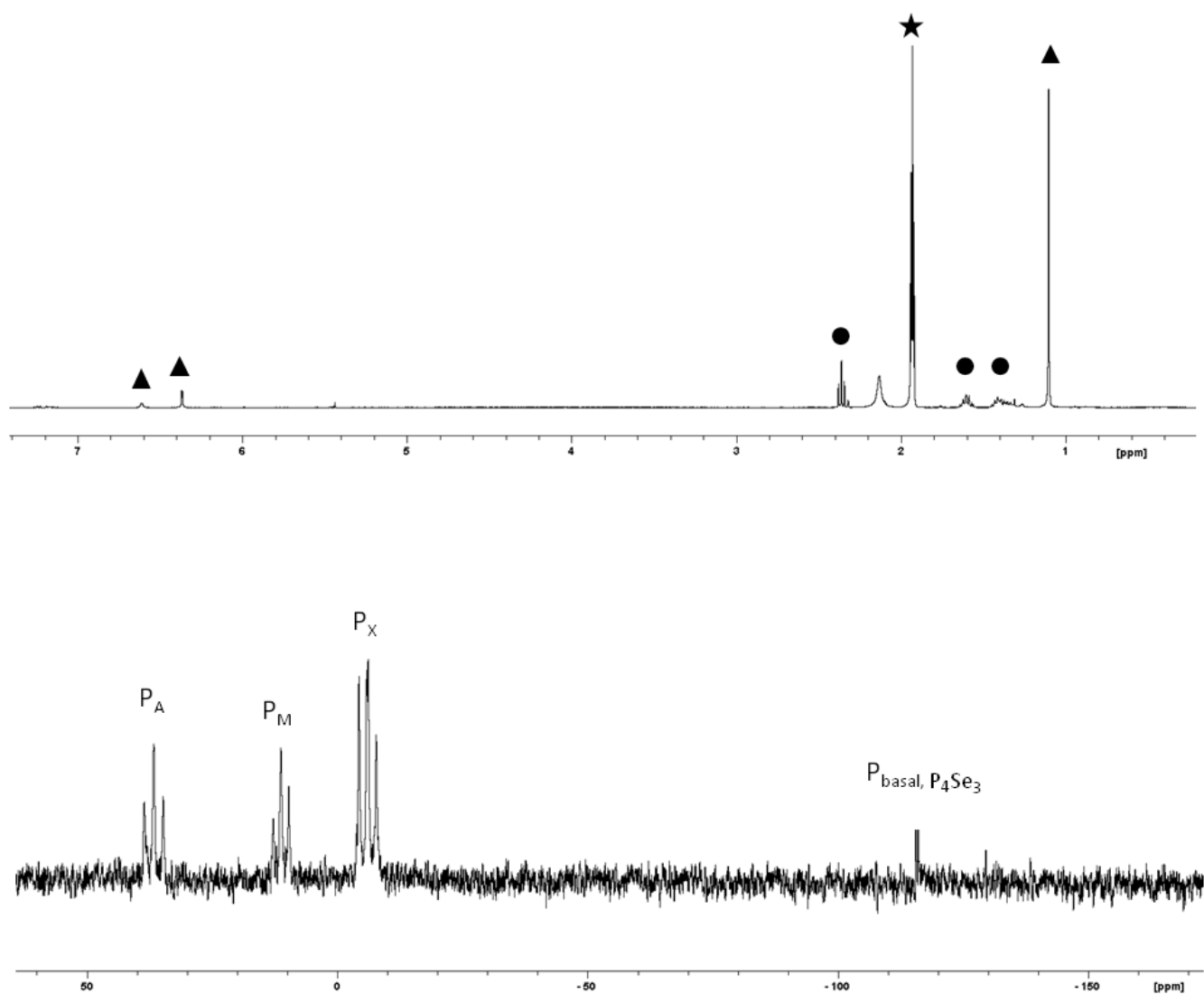


Fig. S2: ¹H NMR spectrum of **7** (top) and ³¹P NMR spectrum of **7** (bottom) in CD₃CN. Symbols ▲, ● and ★ denote signals of **1a**, NC(CH₂)₇CN and of CD₃CN.

4. X-ray Crystallography

Crystals of **5**, **6** and **7** were taken from a Schlenk flask under a stream of argon and immediately covered with perfluorinated Fomblin® mineral oil to prevent both decomposition and a loss of solvent. The quickly chosen single crystals covered by a thin layer of the oil were taken to the pre-centered goniometer head with suitable CryoMount® and directly attached to the goniometer into a stream of cold nitrogen. To collect diffraction data for **7** at the DESY PETRA III synchrotron, the crystals were carefully selected, mounted on a magnetic holder, checked for quality and placed into a Dewar vessel with liquid nitrogen using standard cryocrystallography tools. The X-ray diffraction study of **7** faced many challenges, as the crystals were systematically twinned and quickly decomposed due to the loss of solvent.

The data for **5** and **6** were collected using 1° (**5**) or 0.5° (**6**) ω scans on a Rigaku Oxford Diffraction diffractometer equipped with a Titan^{S2} CCD detector and a SuperNova CuK α microfocus source. The measurements of **5** and **6** were performed at 90 K.

Using standard procedures crystals of **7** were placed into a special Dewar vessel filled with liquid nitrogen among other crystals in the P11 hutch. A robotic mounting/demounting was used for further manipulations. The data for **7** were collected at 80 K at P11 beamline of PETRA III (DESY, Hamburg)^[3] on a 1-axis goniostat using 360°-rotation around ϕ with using 18 keV synchrotron radiation ($\lambda = 0.6888 \text{ \AA}$, 10% transmission) and shutterless data acquisition with 60 ms per 0.2° scan registered with DECTRIS PILATUS 6M photon counting detector. Despite all precautions (attenuated beam, fast measurement) the crystals of **7** proved prone to severe radiation damage, probably due to Ag and Ta absorption (Fig. S3). Various attempts were made to improve data for the refinement: first 700, 1000, 1600 frames were only taken into account to maximally exclude crystal decay. However, this strategy returned low completeness of data for this triclinic structure. The best result was obtained when crystal decay was taken into account for all obtained dataset acceptable providing data completeness of 94%.

The correction of the diffraction data for the radiation damage was done by refining of B -factor (Fig. S3) using CrysAlis PRO software, version 1.171.41.21a.^[4] The correction factor S is computed as follows:

$$S = \exp(B \cdot (\sin(\Theta)/\lambda)^2), \text{ where } \Theta = \text{diffraction angle theta } (^\circ) \text{ and } \lambda = \text{wavelength } (\text{\AA}).$$

The data processing and reduction was performed with CrysAlis PRO Software. The structures were solved by direct methods with *SHELX97* and refined by full-matrix least-squares method on $|F|^2$ using multiprocessor and variable memory version *SHELXL2014*.^[5] Most ordered non-hydrogen atoms were refined in an anisotropic approximation, while the disordered atoms with occupancy factors less than 0.5 were refined isotropically. However, objective limitations of the dataset did not allow anisotropic refinement for some light atoms (N, C, O) due to the unresolved disorder. The hydrogen atoms were refined as riding on pivot atoms. The majority of SbF_6^- counter anions though localized to exactly to fit the charge balance was only possible using rigid body refinement due to severe disorder (s.o.f of the Sb positions vary from ~ 0.015 to 1). The initial geometry obtained by averaging of Sb-F distances in crystal structure determinations at 100 K

containing SF_6^- counter anions, JABVAN and MEJJIW.^[6] An ideal octahedron with Sb-F average bond lengths of 1.872 Å and idealized F-Sb-F angles of 90° was used for the fit. However, the positions of F atoms for total 1/6 SbF_6^- anion per asymmetric unit were not localized, as rigid body model could not be refined properly. Analogously, rigid body refinement for the guest molecule was attempted with the use of the molecular geometry from crystal structure determination^[7] (RefCode SIDSUT03) at 100 K. However, no advantages compared to free refinement was achieved.

Crystallographic data and details of the diffraction experiments are given in Table S1, bond lengths and angles are listed in Tables S2-S4, and molecular structures 5-7 are depicted in Figs. S4-S10. The figures are made in PovRay.^[8]

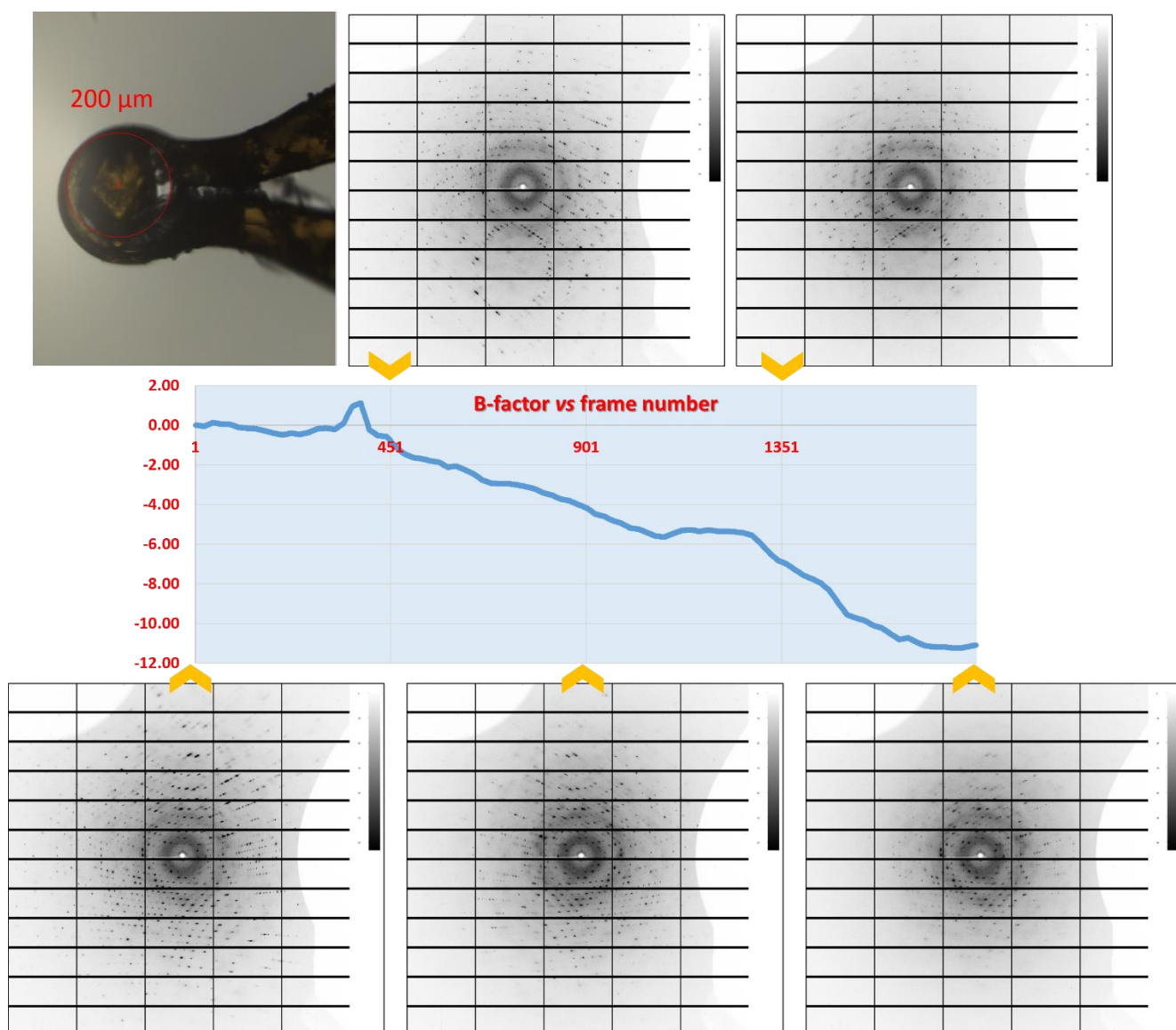


Fig. S3. The variation of *B*-factor vs frame number and corresponding change in the diffraction pattern (ALBULA Viewer v.3.3.0, ©Dectris Ltd., 2014) for a crystal of 7.

CIF files with comprehensive information on the details of the diffraction experiments and full tables of bond lengths and angles for 5, 6 and 7 are deposited in Cambridge Crystallographic Data Centre under the deposition codes CCDC-2009904, CCDC-2009905 and CCDC-2009906, respectively.

Table S1. Crystallographic details for 5, 6 and 7.

Crystal data	5	6	7
CCDC Deposition Code	CCDC-2009904	CCDC-2009905	CCDC-2009906
Structural formula	$[\{\text{Cp}''\text{Ta}(\text{CO})_2(\text{P}_4)\}_2\text{Ag}](\text{SbF}_6) \cdot 0.35(\text{CH}_2\text{Cl}_2)$	$[\{\text{Cp}''\text{Ta}(\text{CO})_2(\text{P}_4)\}_2\text{Ag}](\text{SbF}_6)$	$(\text{P}_4\text{Se}_3)@[\{\text{Cp}''\text{Ta}(\text{CO})_2\}_8\text{Ag}_8(\text{NC}(\text{CH}_2)_7\text{CN})_{4.5}](\text{SbF}_6)_8 \cdot 3.75(\text{CH}_2\text{Cl}_2)$
Chemical formula	$\text{C}_{30.35}\text{H}_{42.70}\text{AgCl}_{0.70}\text{F}_6\text{O}_4\text{P}_8\text{SbTa}_2$	$\text{C}_{15}\text{H}_{21}\text{AgF}_6\text{O}_2\text{P}_4\text{SbTa}$	$\text{C}_{328.5}\text{H}_{477}\text{N}_{18}\text{O}_{32}\text{F}_{96}\text{P}_{72}\text{Cl}_{15}\text{Ag}_{16}\text{Sb}_{16}\text{Ta}_{16}\text{Se}_6$
M_r	1449.64	881.77	16818.72
Crystal system, space group	Triclinic, $P\bar{1}$	Tetragonal, $P4_12_12$	Triclinic, $P\bar{1}$
Temperature (K)	90	90	80
a, b, c (Å)	10.4796(5), 14.2670(6), 17.0118(8)	19.22628 (9), 26.5819 (2)	17.95492(12), 22.56350(18), 38.3495(4)
α, β, γ (°)	96.742(4), 90.464(4), 101.225(4)	90, 90, 90	81.1581(7), 78.4160(7), 73.7720(6)
V (Å ³)	2476.3(2)	9825.98 (13)	14534.6(2)
Z	2	16	2
$F(000)$	1373	6592	7969
D_x (Mg m ⁻³)	1.944	2.384	1.921
Radiation type	Cu $K\alpha$	Cu $K\alpha$	synchrotron ($\lambda = 0.68880$ Å)
μ (mm ⁻¹)	18.58	25.99	4.54
Crystal shape	Rod	Octahedron	Prism
Colour	Orange	Orange	Orange
Crystal size (mm)	0.19 × 0.05 × 0.03	0.07 × 0.05 × 0.04	0.20 × 0.15 × 0.15
Data collection			
Diffractometer	SuperNova, Titan ^{S2}	SuperNova, Titan ^{S2}	P11 beamline, PETRA III, DESY
Absorption correction	Gaussian	Gaussian	Empirical, based on equivalents
T_{\min}, T_{\max}	0.233, 0.759	0.306, 0.544	0.691, 1.000
No. of measured, independent and observed [$I > 2s(I)$] reflections	17168, 9589, 6812	21541, 9807, 8563	144092, 51920, 43562
R_{int}	0.052	0.036	0.068
$(\sin \theta/\lambda)_{\text{max}}$ (Å ⁻¹)	0.627	0.627	0.610
Range of h, k, l	$h = -11 \rightarrow 13, k = -17 \rightarrow 16, l = -15 \rightarrow 21$	$h = -16 \rightarrow 23, k = -22 \rightarrow 21, l = -23 \rightarrow 32$	$h = -21 \rightarrow 21, k = -27 \rightarrow 27, l = -46 \rightarrow 46$
Refinement			
$R[F^2 > 2s(F^2)], wR(F^2), S$	0.067, 0.182, 1.00	0.030, 0.062, 0.95	0.090, 0.287, 1.09
No. of reflections	9589	9807	51920
No. of parameters	511	553	2830
No. of restraints	2	0	127
H-atom treatment	H-atom parameters constrained	H-atom parameters constrained	H-atom parameters constrained
$\Delta\rho_{\text{max}}, \Delta\rho_{\text{min}}$ (e Å ⁻³)	5.62, -1.08	1.10, -1.22	2.68, -4.68
Absolute structure parameter	-	-0.009(5)	-

Computer programs: *CrysAlis PRO* 1.171.39.37b (Rigaku OD, 2017), *SHELXL2015/3* (Sheldrick, 2015), *SHELXL2014/7* (Sheldrick, 2014); *SHELXT2018/5* (Sheldrick, 2018), *SHELXL2018/3* (Sheldrick, 2018).

4.1. One-Dimensional Polymer $[\{\text{Cp}''\text{Ta}(\text{CO})_2(\mu_3, \eta^4: \eta^1: \eta^1\text{-P}_4)\}_2\text{Ag}]_n(\text{SbF}_6)_n \cdot 0.35n(\text{CH}_2\text{Cl}_2)$ (**5**)

In **5** (Fig. S4, S5) one of two crystallographically unique SbF_6^- counter anions is disordered over two close positions. Also one of the tBu groups is disordered over two positions with 0.55/0.45 occupancies (Fig. S4a).

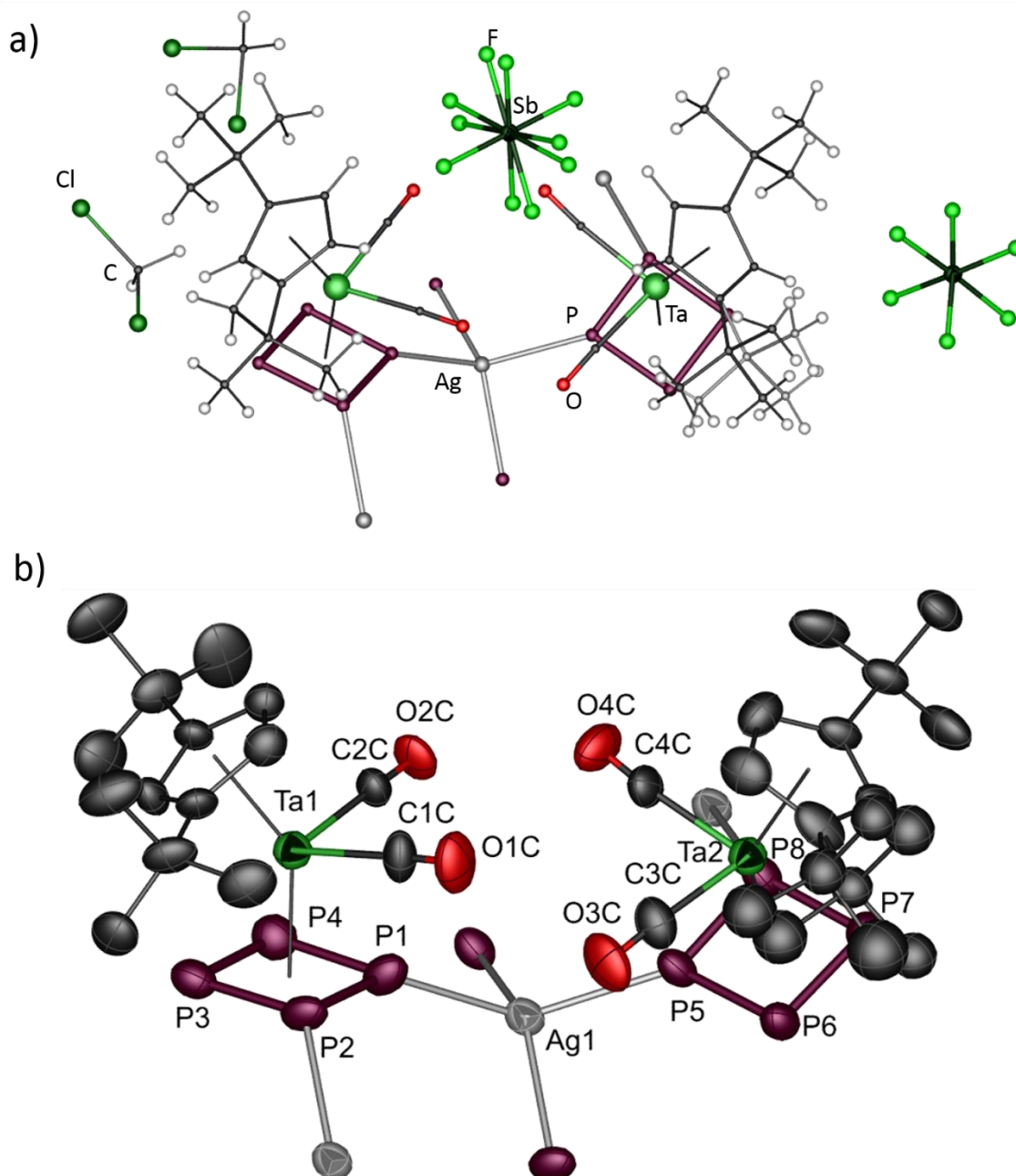


Fig. S4. Asymmetric unit and enumeration scheme in the cationic part of **5**: (a) ball-and-stick and (b) ORTEP (a.d.p. ellipsoids at 50% probability) representations.

Table 2S. Selected geometric parameters (Å, °) for **5**.

Ta1—P3	2.596 (4)	P8—Ag1 ⁱⁱ	2.563 (3)
Ta1—P2	2.611 (3)	P1—P2	2.166 (5)
Ta1—P1	2.629 (3)	P1—P4	2.179 (5)
Ta1—P4	2.650 (4)	P2—P3	2.179 (5)
Ta2—P8	2.606 (3)	P3—P4	2.155 (5)
Ta2—P7	2.615 (3)	P5—P8	2.149 (5)
Ta2—P5	2.644 (3)	P5—P6	2.165 (4)
Ta2—P6	2.652 (3)	P6—P7	2.155 (5)
Ag1—P5	2.494 (3)	P7—P8	2.166 (4)
Ag1—P1	2.511 (3)	O1C—C1C	1.115 (16)
Ag1—P2 ⁱ	2.551 (3)	O2C—C2C	1.094 (15)
Ag1—P8 ⁱⁱ	2.563 (3)	O3C—C3C	1.141 (17)
P2—Ag1 ⁱ	2.551 (3)	O4C—C4C	1.113 (15)
P1—Ag1—P2 ⁱ	101.72 (11)	P5—Ag1—P1	134.73 (13)
P1—Ag1—P8 ⁱⁱ	90.33 (11)	P5—Ag1—P2 ⁱ	94.58 (11)
P2 ⁱ —Ag1—P8 ⁱⁱ	140.49 (12)	P5—Ag1—P8 ⁱⁱ	103.28 (11)

Symmetry codes: (i) $-x, -y, -z+1$; (ii) $-x+1, -y, -z+1$.

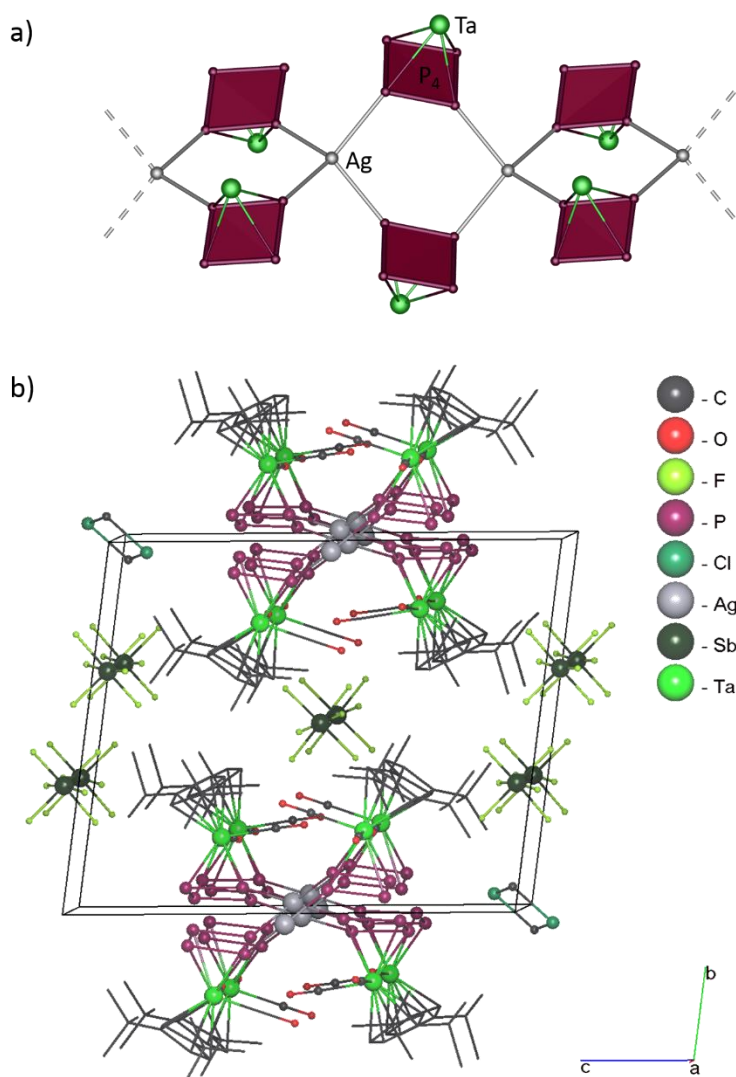


Fig. S5. The coordination motif in **5** based on Ag_2P_4 six-membered cycles (a) and crystal packing (b). H atoms are not shown for clarity.

4.2. Three-Dimensional Polymer $[\{\text{Cp}''\text{Ta}(\text{CO})_2(\mu_4, \eta^4:\eta^1:\eta^1:\eta^1\text{-P}_4)\}_2\text{Ag}]_n(\text{SbF}_6)_n$ (**6**)

On the contrary to **5**, the crystal structure of **6** is solvent-free. Unlike **5**, counter anions SbF_6^- and $t\text{Bu}$ groups of the Cp'' ligands are all ordered (Fig. S6-S8).

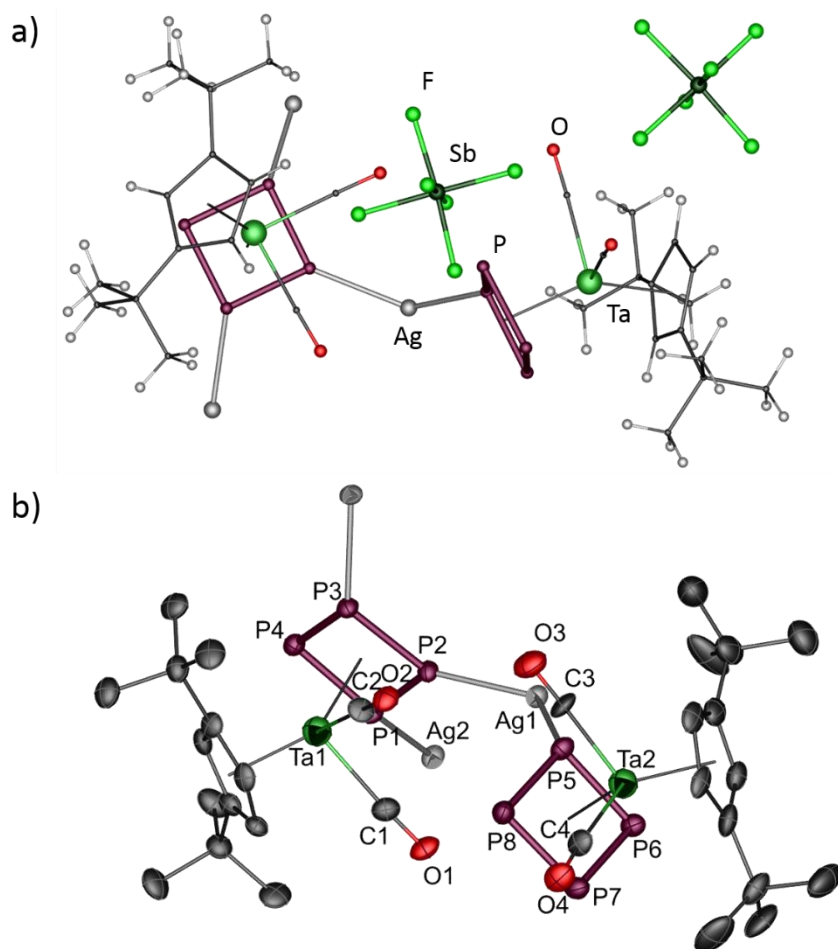


Fig. S6. Asymmetric unit and enumeration scheme in **6**: (a) ball-and-stick and (b) ORTEP (ellipsoids at 50% probability) representations.

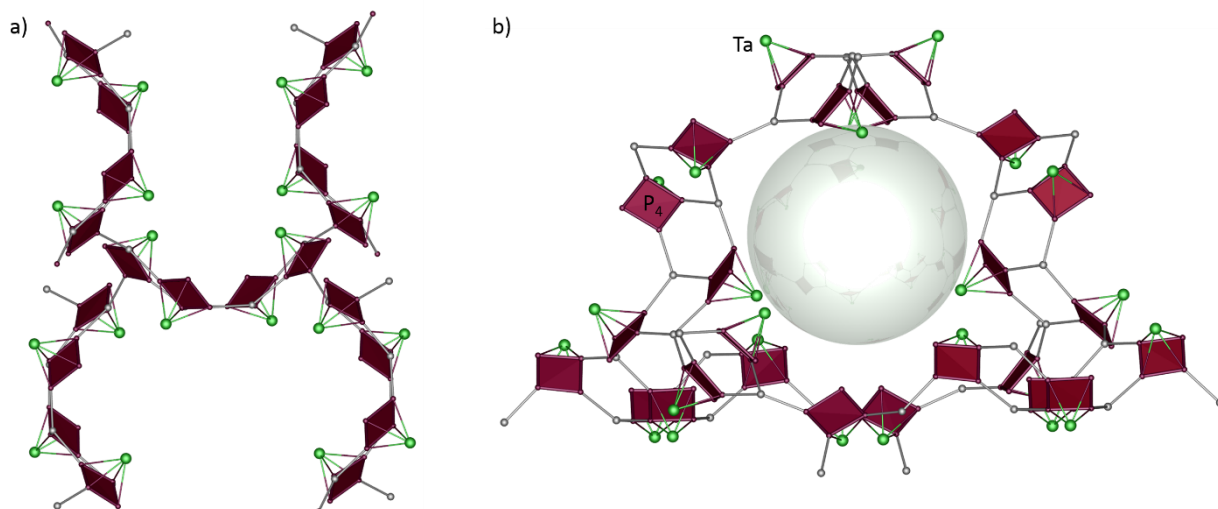


Fig. S7. (a) A section of 3D framework in **6**. (b) A void in the framework of **6** visualised by a hypothetical ball of 11 Å in diameter.

Table S3. Selected geometric parameters (Å, °) for 6

Ta1—P1	2.595 (2)	C11—C12	1.414 (14)
Ta1—P2	2.663 (3)	C11—C15	1.426 (14)
Ta1—P3	2.606 (3)	C11—C111	1.539 (13)
Ta1—P4	2.635 (3)	C12—C13	1.440 (13)
Ta1—C1	2.131 (10)	C13—C14	1.389 (15)
Ta1—C2	2.104 (9)	C13—C131	1.533 (13)
Ta1—C11	2.395 (9)	C14—C15	1.421 (13)
Ta1—C12	2.373 (9)	C21—C22	1.424 (17)
Ta1—C13	2.389 (9)	C21—C25	1.428 (14)
Ta1—C14	2.382 (9)	C21—C211	1.519 (17)
Ta1—C15	2.381 (10)	C22—C23	1.439 (16)
Ta2—P5	2.609 (3)	C23—C24	1.425 (17)
Ta2—P6	2.591 (2)	C23—C231	1.51 (2)
Ta2—P7	2.606 (3)	C24—C25	1.395 (18)
Ta2—P8	2.681 (3)	C111—C112	1.517 (16)
Ta2—C3	2.115 (9)	C111—C113	1.528 (15)
Ta2—C4	2.121 (10)	C111—C114	1.531 (15)
Ta2—C21	2.390 (11)	C131—C132	1.538 (15)
Ta2—C22	2.354 (10)	C131—C133	1.515 (15)
Ta2—C23	2.377 (12)	C131—C134	1.526 (16)
Ta2—C24	2.393 (11)	C211—C212	1.525 (16)
Ta2—C25	2.407 (10)	C211—C213	1.527 (19)
P1—P2	2.154 (3)	C211—C214	1.55 (2)
P1—P4	2.170 (3)	C231—C232	1.53 (2)
P2—P3	2.149 (3)	C231—C233	1.535 (19)
P3—P4	2.159 (3)	C231—C234	1.54 (2)
P5—P6	2.146 (3)	Ag1—P2	2.465 (3)
P5—P8	2.180 (4)	Ag1—P5	2.456 (3)
P6—P7	2.140 (4)	Ag1—P6 ⁱⁱ	2.485 (2)
P7—P8	2.170 (4)	Ag2—P1	2.455 (2)
C1—O1	1.126 (12)	Ag2—P3 ⁱⁱⁱ	2.446 (3)
C2—O2	1.127 (11)	Ag2—P7 ⁱⁱ	2.493 (3)
C3—O3	1.118 (12)	P6—Ag1 ⁱⁱ	2.485 (2)
C4—O4	1.121 (13)	P3—Ag2 ⁱ	2.446 (2)
		P7—Ag2 ⁱⁱ	2.493 (3)
P2—Ag1—P6 ⁱⁱ	103.38 (8)	Ag1—P2—Ta1	125.67 (11)
P5—Ag1—P2	127.36 (9)	Ag1—P5—Ta2	162.00 (13)
P5—Ag1—P6 ⁱⁱ	116.68 (8)	Ag1 ⁱⁱ —P6—Ta2	155.79 (12)
P1—Ag2—P7 ⁱⁱ	106.28 (8)	Ag2 ⁱⁱ —P7—Ta2	145.37 (12)
P3 ⁱⁱⁱ —Ag2—P1	130.47 (9)	P3—P4—P1	89.66 (13)
P3 ⁱⁱⁱ —Ag2—P7 ⁱⁱ	121.05 (9)	P2—P1—P4	89.71 (12)
O1—C1—Ta1	176.6 (10)	P2—P3—P4	90.13 (13)
O2—C2—Ta1	178.6 (8)	P3—P2—P1	90.32 (13)
O3—C3—Ta2	178.0 (11)	P6—P5—P8	90.39 (14)
O4—C4—Ta2	175.8 (9)	P7—P6—P5	90.23 (13)
Ag2—P1—Ta1	149.68 (11)	P6—P7—P8	90.83 (14)
Ag2 ⁱ —P3—Ta1	153.68 (11)	P7—P8—P5	88.53 (14)

Symmetry codes: (i) $y-1/2, -x-1/2, z-1/4$; (ii) $-y, -x, -z+5/2$; (iii) $-y-1/2, x+1/2, z+1/4$.

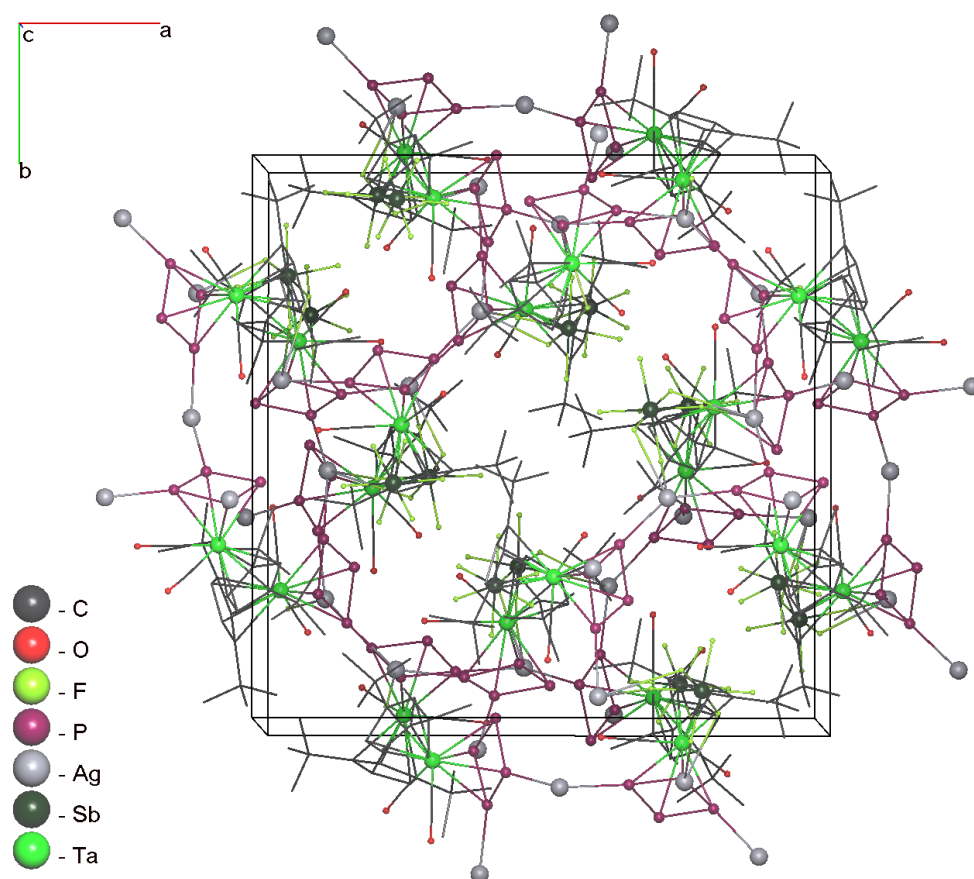


Fig. S8. A crystal packing in **6**. H atoms are not shown for clarity.

4.3. Two-Dimensional Coordination Network $P_4Se_3@[\{(Cp''Ta(CO)_2(\eta^4-P_4))Ag\}_8(NC(CH_2)_7CN)_{4.5}]_n[SbF_6]_{8n} \cdot 3.75n(CH_2Cl_2)$ (**7**)

Due to objectively restricted quality of the diffraction data caused by radiation damage (this is also the reason for imperfect a.d.p. parameters, Fig. 9b), the disorder of the light atoms in the structure is most probably modelled incompletely. The final composition established from X-ray structure analysis is $(P_4Se_3)@[\{(Cp''TaP_4(CO)_2\}_8Ag_8(NC(CH_2)_7CN)_{4.5}][SbF_6]_{8n} \cdot 3.75n(CH_2Cl_2)$, returning reasonable calculated density (Table S1). However, greater number of solvent molecules should be present taking into account low occupancies of the localized ones in every position. Only a few counter anions and solvent molecules are rather ordered, therefore, they are not shown in figures for clarity.

Disorder of the guest:

The guest molecule P_4S_3 completely occupies the cavity of the supramolecular node; it is however disordered over two positions with 80% and 20% occupancies (Fig. S9b). The atoms P1i (occupancy 0.8) and P11i (occupancy 0.2) correspond to the apical positions of the disordered components of the cage molecule, respectively. Se1 and P4i atomic positions is shared between P and Se atoms; Se2 and Se3 belong to both orientations of the molecule. The disorder is most probably occurs due to alternatives in positioning of the guest molecule provided by the geometry of the cavity. The size of the cavity is estimated as the minimal and maximal distance between the centroids of every individual *cyclo*- P_4 unit and the centroid of the node minus twice the van der Waals radius of P ($1.8 \text{ \AA} \times 2$) (Fig. S9a).

The host-guest interactions are mostly of van-der Waals nature ($P \cdots P \geq 3.6 \text{ \AA}$, $P \cdots Se \geq 3.7 \text{ \AA}$), but a number of shortened $P \cdots P$ contacts occurs for both major and minor orientations (Fig. S9b). Also one shortened $P \cdots Se$ contact and two contacts on the border 'van-der-Waals - specific' are found.

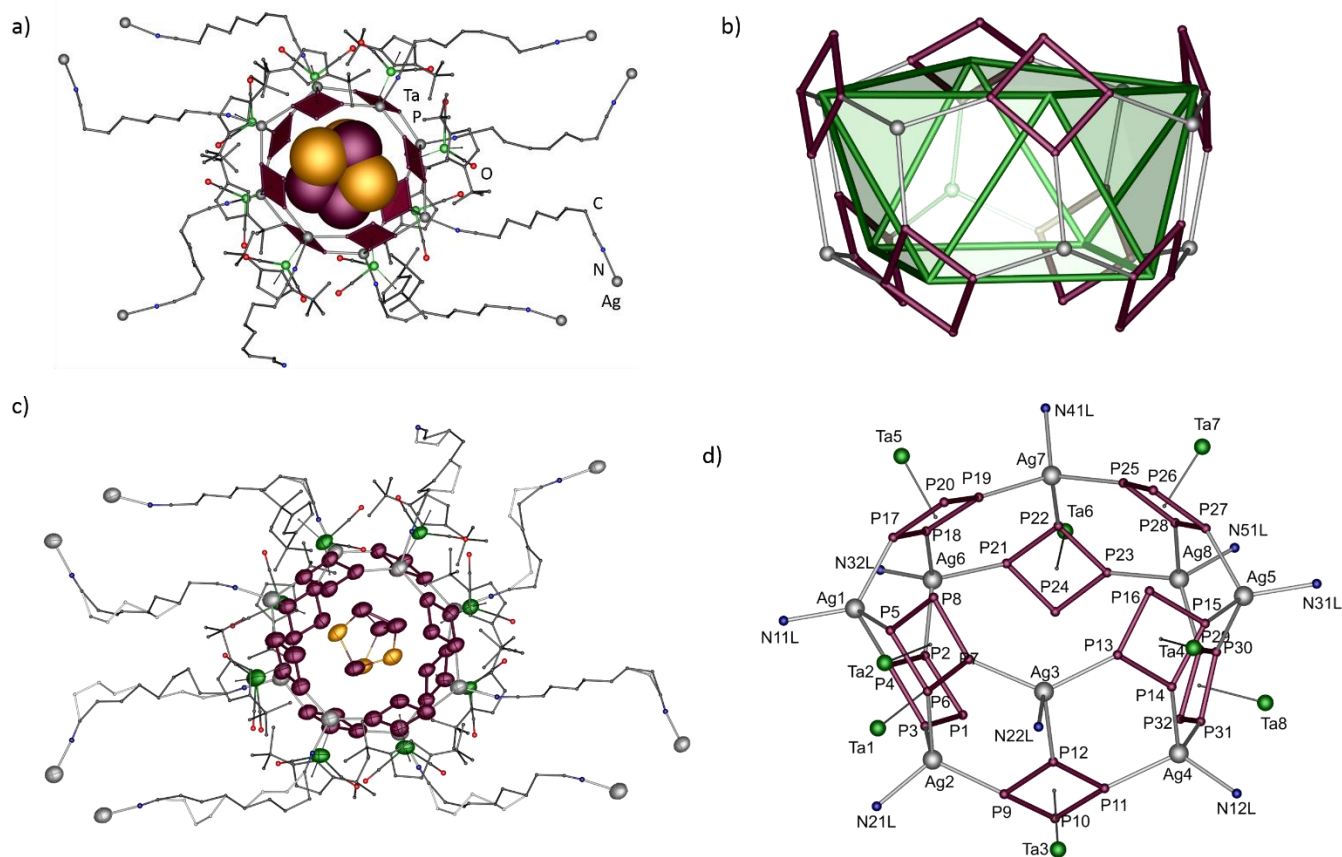


Fig. S9. (a) and (b) Supramolecular node (guest molecule P_4Se_3 is shown in van der Waals spheres), (c) part of the asymmetric unit (a.d.p. ellipsoids for heavy atoms at 50% probability) and (d) enumeration scheme in **7**. Severely disordered SbF_6^- counter anions and solvent molecules are omitted for clarity.

Table S4. Selected geometric parameters (\AA , $^\circ$) for **7**

Se2—P13I	2.033(17)	Se3—P1I—Se2	96.2(2)
Se2—P2I	2.153(6)	Se1—P1I—Se2	97.5(2)
Se2—P1I	2.355(7)	P4I—P2I—Se2	112.9(3)
Se2—P11I	2.391(14)	P4I—P2I—P3I	60.5(2)
Se3—P12I	2.064(16)	Se2—P2I—P3I	109.4(3)
Se3—P3I	2.170(6)	P4I—P3I—Se3	111.2(3)
Se3—P1I	2.266(5)	P4I—P3I—P2I	58.2(2)
Se3—P11I	2.529(15)	Se3—P3I—P2I	104.6(3)
Se1—P1I	2.283(6)	P2I—P4I—P3I	61.2(2)
Se1—P4I	2.365(4)	P2I—P4I—Se1	102.7(2)
P2I—P4I	2.114(6)	P3I—P4I—Se1	102.4(2)
P2I—P3I	2.180(8)	Se1I—P11I—Se2	97.6(5)
P3I—P4I	2.165(6)	Se1I—P11I—Se3	94.6(6)
P11I—Se1I	2.336(14)	Se2—P11I—Se3	88.7(5)
P12I—P14I	1.980(12)	P14I—P12I—Se3	118.2(8)
P12I—P13I	2.156(17)	P14I—P12I—P13I	56.5(5)
P13I—P14I	1.963(13)	Se3—P12I—P13I	111.2(9)
P14I—Se1I	2.365(4)	P14I—P13I—Se2	121.5(8)
Ta1—P3	2.597(3)	P14I—P13I—P12I	57.2(5)
Ta1—P2	2.602(4)	Se2—P13I—P12I	105.1(8)
Ta1—P1	2.614(3)	P13I—P14I—P12I	66.3(5)
Ta1—P4	2.643(3)	P13I—P14I—Se1I	101.0(5)

Ta2—P5	2.58(3)	P12I—P14I—Se1I	104.4(5)
Ta2—P6	2.61(3)	N11L—Ag1—P17	126.5(4)
Ta2—P7	2.62(3)	N11L—Ag1—P5	113.8(6)
Ta2—P8	2.64(3)	N11L—Ag1—P4	105.4(4)
Ta2A—P5	2.58(3)	N12L ⁱ —Ag4—P11	116.9(5)
Ta2A—P6	2.61(3)	N12L ⁱ —Ag4—P31	107.2(4)
Ta2A—P7	2.62(3)	N12L ⁱ —Ag4—P14	106.4(4)
Ta2A—P8	2.64(3)	N21L—Ag2—P9	109.4(5)
Ta3—P9	2.598(4)	N21L—Ag2—P6	110.3(4)
Ta3—P11	2.605(4)	N21L—Ag2—P3	112.8(5)
Ta3—P10	2.635(4)	N22L ⁱⁱⁱ —Ag3—P13	112.2(4)
Ta3—P12	2.647(3)	N22L ⁱⁱⁱ —Ag3—P7	106.5(4)
Ta4—P15	2.596(3)	N22L ⁱⁱⁱ —Ag3—P12	96.9(4)
Ta4—P13	2.620(4)	N31L—Ag5—P15	124.4(3)
Ta4—P16	2.641(4)	N31L—Ag5—P30	113.3(3)
Ta4—P14	2.649(3)	N31L—Ag5—P27	107.0(4)
Ta5—P17	2.595(4)	N32L ⁱⁱ —Ag6—P21	109.2(3)
Ta5—P18	2.605(3)	N32L ⁱⁱ —Ag6—P18	115.9(3)
Ta5—P19	2.634(3)	N32L ⁱⁱ —Ag6—P2	110.1(3)
Ta5—P20	2.676(4)	N41L—Ag7—P25	112.0(3)
Ta6—P21	2.601(3)	N41L—Ag7—P19	110.5(3)
Ta6—P23	2.608(3)	N41L—Ag7—P22	98.3(3)
Ta6—P24	2.638(3)	N51L—Ag8—P23	110.9(3)
Ta6—P22	2.650(3)	N51L—Ag8—P29	114.4(3)
Ta7—P27	2.615(3)	N51L—Ag8—P28	99.7(3)
Ta7—P25	2.621(3)	P17—Ag1—P5	103.28(15)
Ta7—P26	2.638(3)	P17—Ag1—P4	103.96(12)
Ta7—P28	2.659(3)	P5—Ag1—P4	100.56(13)
Ta8—P29	2.594(3)	P9—Ag2—P6	104.44(13)
Ta8—P31	2.609(3)	P9—Ag2—P3	119.06(13)
Ta8—P32	2.640(3)	P6—Ag2—P3	99.76(12)
Ta8—P30	2.641(3)	P13—Ag3—P7	127.42(14)
Ag1—N11L	2.179(17)	P13—Ag3—P12	101.50(12)
Ag2—N21L	2.248(18)	P7—Ag3—P12	107.71(12)
Ag3—N22L ⁱⁱⁱ	2.253(16)	P11—Ag4—P31	116.96(11)
Ag4—N12L ⁱ	2.253(14)	P11—Ag4—P14	102.62(12)
Ag5—N31L	2.230(14)	P31—Ag4—P14	105.59(11)
Ag6—N32L ⁱⁱ	2.241(11)	P15—Ag5—P30	99.51(12)
Ag7—N41L	2.305(14)	P15—Ag5—P27	111.90(13)
Ag8—N51L	2.277(12)	P30—Ag5—P27	97.34(11)
Ag1—P4	2.553(3)	P21—Ag6—P18	105.79(10)
Ag1—P5	2.502(5)	P21—Ag6—P2	114.90(11)
Ag1—P17	2.494(4)	P18—Ag6—P2	100.79(12)
Ag2—P3	2.501(4)	P25—Ag7—P19	123.41(11)
Ag2—P6	2.496(4)	P25—Ag7—P22	105.30(9)
Ag2—P9	2.479(4)	P19—Ag7—P22	103.60(10)
Ag3—P7	2.507(4)	P23—Ag8—P29	119.84(11)
Ag3—P13	2.498(4)	P23—Ag8—P28	105.46(9)
Ag3—P12	2.583(3)	P29—Ag8—P28	103.70(10)
Ag4—P11	2.478(4)	P2—P1—P3	90.61(18)
Ag4—P31	2.525(3)	P1—P2—P4	89.4(2)
Ag4—P14	2.561(3)	P1—P3—P4	89.6(2)
Ag5—P15	2.479(4)	P3—P4—P2	90.27(18)
Ag5—P30	2.528(3)	P8—P5—P6	89.5(2)
Ag5—P27	2.531(3)	P7—P6—P5	90.8(2)
Ag6—P21	2.485(3)	P6—P7—P8	89.3(2)
Ag6—P18	2.503(3)	P5—P8—P7	90.3(2)
Ag6—P2	2.527(4)	P10—P9—P12	90.8(2)
Ag7—P25	2.485(3)	P9—P10—P11	89.62(18)
Ag7—P19	2.496(3)	P10—P11—P12	90.4(2)
Ag7—P22	2.574(3)	P9—P12—P11	89.13(18)
Ag8—P23	2.477(3)	P14—P13—P16	90.2(2)

Ag8—P29	2.485(3)	P13—P14—P15	89.98(19)
Ag8—P28	2.575(3)	P16—P15—P14	90.1(2)
P1—P2	2.150(5)	P15—P16—P13	89.7(2)
P1—P3	2.151(5)	P18—P17—P20	93.63(19)
P2—P4	2.160(5)	P17—P18—P19	87.58(17)
P3—P4	2.154(5)	P18—P19—P20	92.49(18)
P5—P8	2.151(7)	P17—P20—P19	86.27(17)
P5—P6	2.161(6)	P22—P21—P24	90.00(15)
P6—P7	2.145(5)	P23—P22—P21	89.85(15)
P7—P8	2.174(6)	P22—P23—P24	90.40(15)
P9—P10	2.143(5)	P23—P24—P21	89.66(15)
P9—P12	2.152(5)	P28—P25—P26	90.56(16)
P10—P11	2.151(5)	P27—P26—P25	89.71(17)
P11—P12	2.161(5)	P26—P27—P28	90.52(17)
P13—P14	2.147(5)	P25—P28—P27	89.17(16)
P13—P16	2.161(5)	P30—P29—P32	90.05(16)
P14—P15	2.157(5)	P29—P30—P31	90.78(16)
P15—P16	2.155(5)	P30—P31—P32	89.64(16)
P17—P18	2.131(5)	P29—P32—P31	89.41(15)
P17—P20	2.158(5)		
P18—P19	2.153(5)		
P19—P20	2.177(5)		
P21—P22	2.165(4)		
P21—P24	2.165(4)		
P22—P23	2.154(4)		
P23—P24	2.161(4)		
P25—P28	2.150(4)	P-P range, average	2.131(5)-2.177(5), 2.16[1]
P25—P26	2.158(5)	Ag-P range, average	2.477(3)-2.583(3), 2.51[3]
P26—P27	2.141(4)	Ag-N range, average	2.179(17)-2.305(14), 2.25[4]
P27—P28	2.169(5)		
P29—P30	2.138(4)	P-Ag-P range, average	97.34(11)-127.42(14), 108[8]
P29—P32	2.158(4)	N-Ag-P range, average	96.9(4)-126.5(4), 110[6]
P30—P31	2.141(4)	P-P-P range, average	86.27(17)-93.63(19), 90[1]
P31—P32	2.171(4)		

Symmetry codes: (i) $x, y-1, z$; (ii) $x, y+1, z$; (iii) $-x+2, -y+1, -z$.

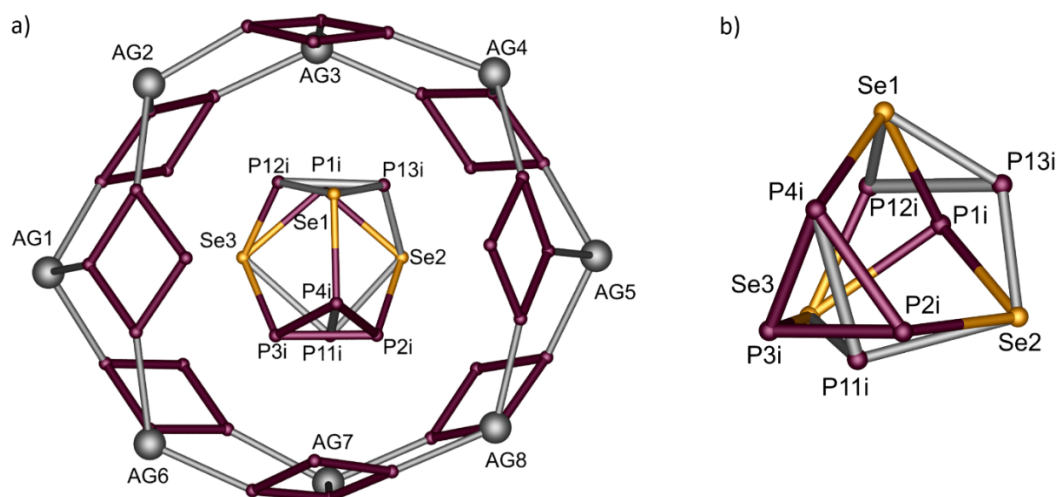


Fig. S10. The disorder model of (b) the guest molecule P₄Se₃ in the cavity of (a) supramolecule 7. Major component (80%) is shown in colour, the minor one (20%) in grey.

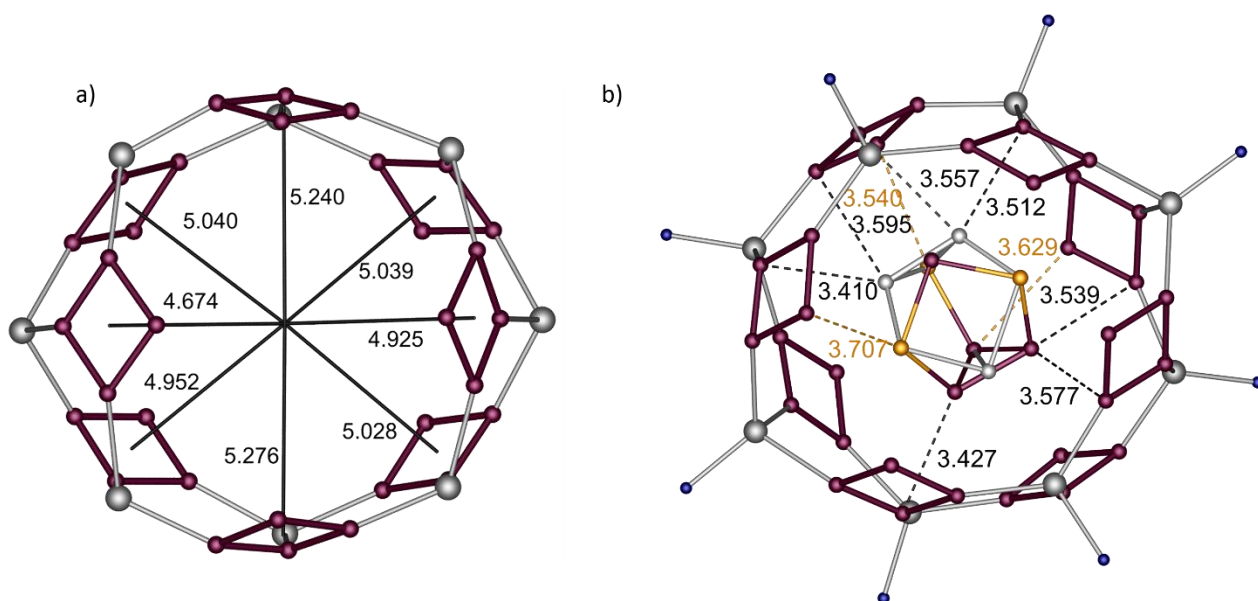


Fig. S11. (a) An estimation of the cavity size and (b) shortest host-guest interactions between *cyclo*-P₄ and P₄Se₃ in **7**.

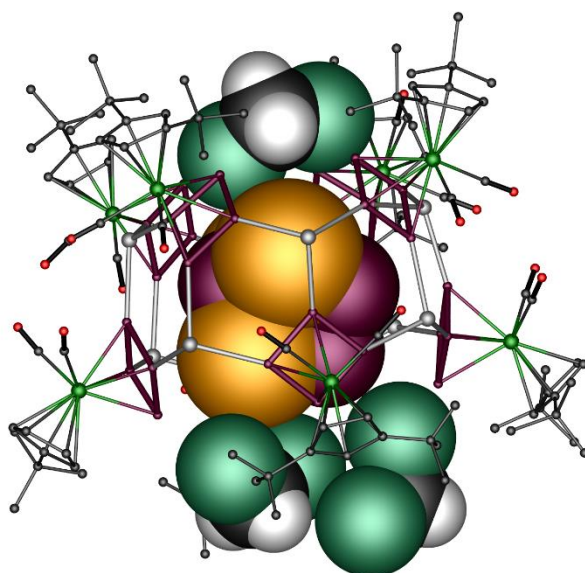


Fig. S12. The solvent molecules captured among the Cp'' ligands of **1a** and blocking the portals of the barrel-like node in **7**. Solvent molecules CH₂Cl₂ and guest molecule P₄Se₃ is shown in van der Waals spheres.

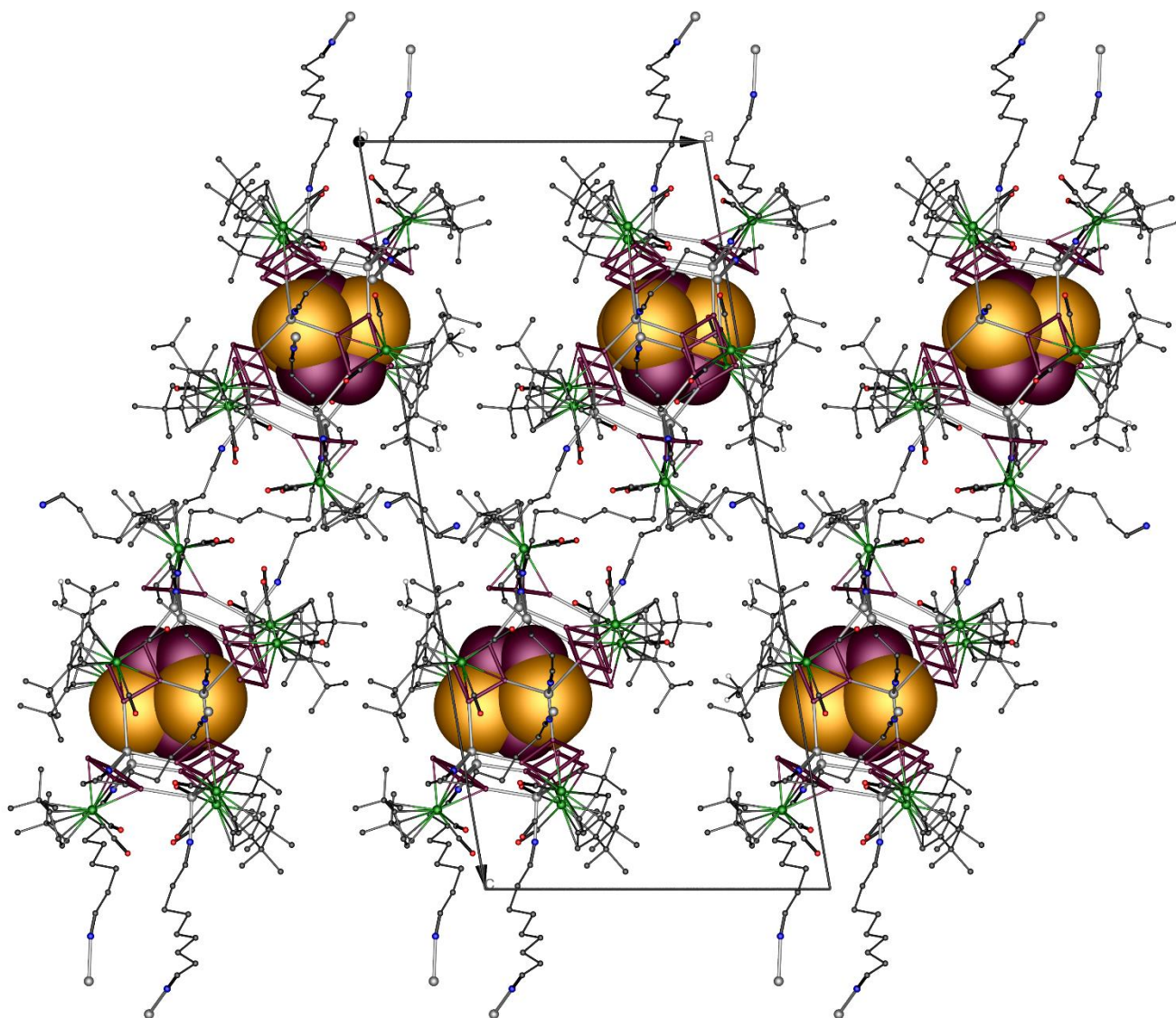


Fig. S13. The packing of polymeric layers in the plane *ab* for **7**. Solvent molecules CH_2Cl_2 and severely disordered SbF_6^- counter anions in-between the layers are not shown. The guest molecules P_4Se_3 are shown in van der Waals spheres.

5. Topological Features of the Coordination Networks **6** and **7**

For simpler representation of the connectivity in the coordination compounds **6** and **7**, we performed topological simplification and classification of the underlying nets with TOPOSPro software⁹. In **6**, we considered every tetrameric units $\{\text{Ag}_4(\mathbf{1a})_4\}$ as nodes and a Ag-P bonds connecting tetramers as spacers in the corresponding underlying net and analysed its topology. The resulting net possesses the topology of a diamond structure, **dia** (Fig. S14), according to the database of topological types RCSR.^{9c} Analogously, the simplification of the network in **7** was performed. The nodes were defined as $\{\text{Ag}_8(\mathbf{1a})_8\}$ supramolecular nodes, and bridging dinitrile linkers were considered as spacers. Terminal dinitriles do not influence on the connectivity of the network and are ignored for this reason. The calculated topology of a 2D net was determined as Shubnikov tetragonal plane net, **sql** (square lattice, Fig. S15). Note that all geometrical distortions are always ignored during topological analysis and only connectivity is taken into account. Therefore, rectangular shape of the mesh is considered topologically same as a square.

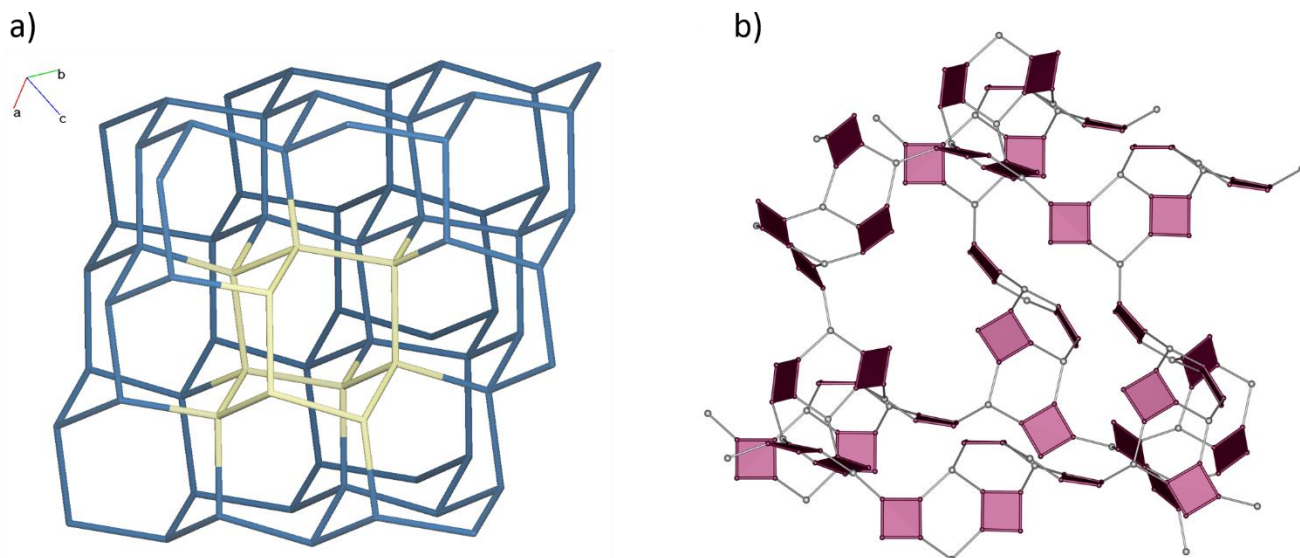


Fig. S14. (a) The underlying net **dia** of $\{\text{Ag}_4(\mathbf{1a})_4\}$ tetramers in crystal structure of **6** with one diamond-like cage highlighted in orange and presented (b) as a part of non-simplified structure presented as Ag-P₄ ligand framework. $\{\text{Cp}''\text{Ta}(\text{CO})_2\}$ fragments are not shown for clarity.

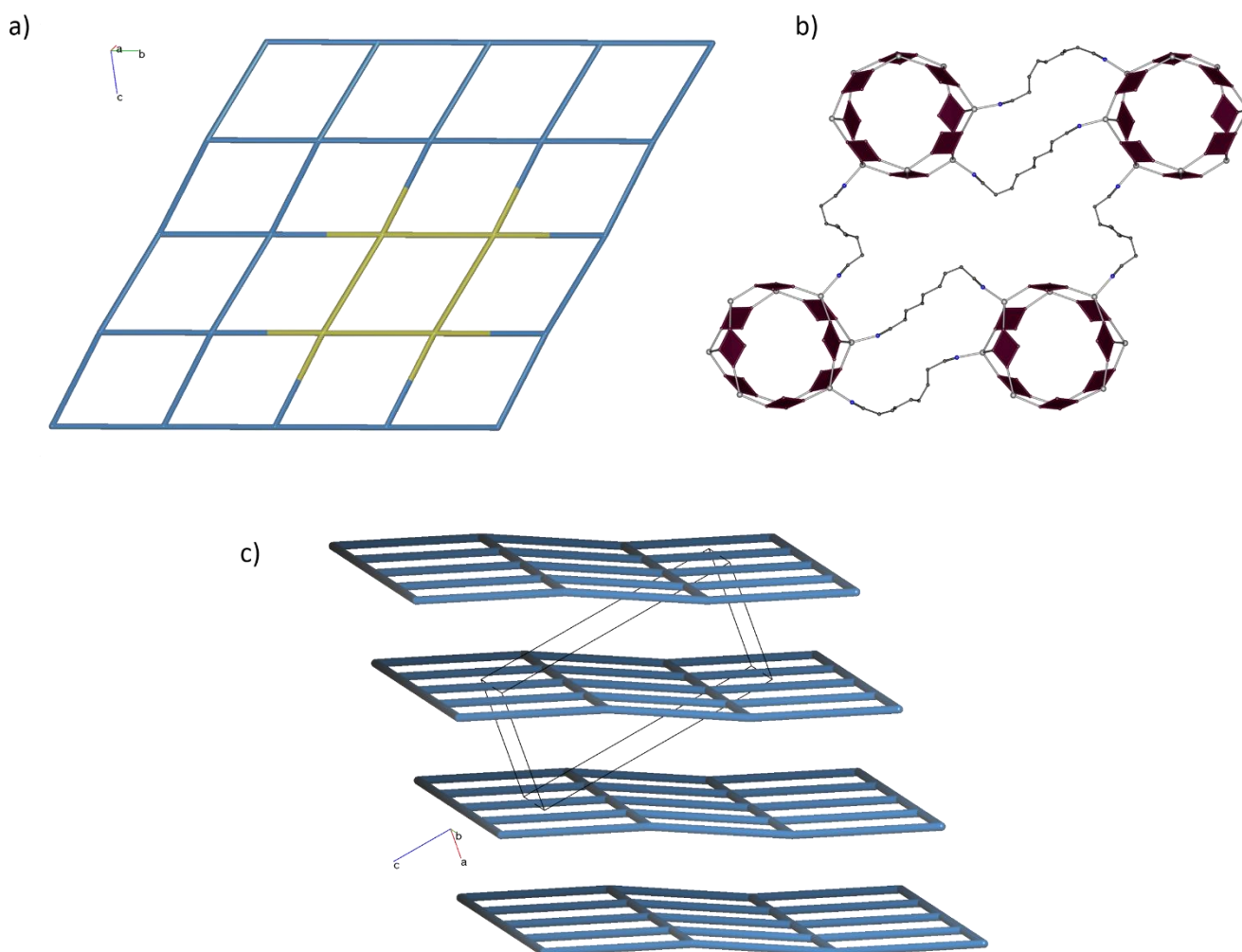


Fig. S15. (a) The underlying net **sql** of supramolecules $\{\text{Ag}_8(\mathbf{1a})_8\}$ in crystal structure of **7**. One 'square' mesh is as a part of non-simplified structure presented as Ag-P₄ ligand framework. $\{\text{Cp}''\text{Ta}(\text{CO})_2\}$ fragments are not shown for clarity. (c) The packing of the planar underlying nets **sql** in crystal structure of **7**.

References

- [1] O. J. Scherer, R. Winter, G. Wolmershäuser, *Z. Anorg. Allg. Chem.* **1993**, *619*, 827-835.
- [2] E. Keulen and A. Vos, *Acta Cryst.*, 1959, **12**, 323.
- [3] A. Burkhardt, T. Pakendorf, B. Reime et al, *Eur. Phys. J. Plus* **131**, 56-64 (2016).
- [4] *CrysAlisPRO*, different versions 2006-2020, Rigaku Oxford Diffraction.
- [5] G. M. Sheldrick, *Acta Cryst. sect. C.*, **2015**, *C71*, 3.
- [6] C. R. Groom, I. J. Bruno, M. P. Lightfoot and S. C. Ward, *Acta Cryst.* **2016**, *B72*, 171-179.
- [7] P. Weis, I. Krossing, D. Kratzert, C. Hettich, *Eur. J. Inorg. Chem.*, **2019**, 1657.
- [8] POV-Ray. <https://www.povray.org>
- [9] (a) V. A. Blatov, A. P. Shevchenko and D. M. Proserpio, *Cryst. Growth Des.*, 2014, **14**, 3576; <https://topospro.com> (b) V. A. Blatov, M. O'Keeffe and D. M. Proserpio, *CrystEngComm* 2010, **12**, 44; (c) M. O'Keeffe, M. A. Peskov, S. J. Ramsden and O. M. Yaghi, *Accts. Chem. Res.*, 2008, **41**, 1782; <http://www.rcsr.net>.